CHEMISTRY

Identifying key intermediates generated in situ from Cu(II) salt–catalyzed C–H functionalization of aromatic amines under illumination

Qing-Yuan Meng,[1] Xue-Wang Gao,[1] Tao Lei,[1] Zan Liu,[1] Fei Zhan,[2] Zhi-Jun Li,[1] Jian-Ji Zhong,[1] Hongyan Xiao,[1] Ke Feng,[1] Bin Chen,[1] Ye Tao,[2] Chen-Ho Tung,[1] Li-Zhu Wu[1]*

Copper compounds involved in photocatalysis have recently spurred considerable interest for their novel transformations. However, mechanistic investigations are still in infancy. We find a new type of reaction, that is, Cu(II) salt–catalyzed C–H functionalization of aromatic amines triggered by visible light irradiation. An array of mechanistic observations, including high-resolution mass spectrometry, ultraviolet-visible absorption spectrum, electron spin resonance, x-ray absorption near-edge structure, and density functional theory calculation, have identified the key intermediates generated in situ in the transformation. Integration of single-electron transfer, singlet oxygen ($^1O_2$), and new absorption species, intermediate I and intermediate II formed in situ from Cu(II) salts and substrate amines or imines, respectively, is responsible for the N–H and C–H bond activation of secondary amines to couple with nucleophiles in air, thereby leading to the formation of quinoline, indolo[3,2-*c*]quinoline, β-amino acid, and 1,4-dihydropyridine derivatives in moderate to good yields under visible light irradiation at room temperature.

INTRODUCTION

Copper salts, which are inexpensive and easily accessible to different oxidation states, have been widely used to activate a variety of C–H bonds for the construction of complex compounds (*1*–*4*). Rapid growth of photocatalysis in recent years has introduced new strategies to make chemical reactions occur efficiently under mild conditions (*5*–*10*). The use of copper complexes as photoredox catalysts has shown promise for C–C or C–X (X = N, O, or Br) bond formation (*11*–*26*). In particular, Ullmann C–N coupling of carbazole with aryl halides could be accomplished at room temperature under ultraviolet (UV) illumination (*27*). In contrast to the well-established photocatalytic systems, the reaction underwent smoothly without external photosensitizers, and Cu(I) ions, instead of copper complexes, directly initiated the photocatalytic reaction. It was supposed that Cu(I) ion interacted with carbazole substrate to form a Cu(I)-N intermediate in situ that was responsive to UV light for further transformation. As a photochemical key step, the electron transfer from the Cu(I)-N intermediate to the halide was proposed. Furthermore, the combination of CuI and light was also effective for the coupling of alkyl and aryl halides with nitrogen, sulfur, and oxygen nucleophiles (*27*–*36*). These stimulating results have revealed the versatile reactivity of copper salts and broad tolerance of functional groups. At the same time, the rapid advances have attracted much interest in monitoring the intermediates generated in situ under illumination.

In this contribution, we report a new type of reaction, where Cu(II) salts, instead of copper complexes or Cu(I) ions, are capable of activating C–H bonds of secondary amines **1** to directly construct a range of C–C bonds in air, leading to the formation of quinoline, indolo[3,2-*c*]quinoline, β-amino acid, and 1,4-dihydropyridine scaffolds in good chemical yields under visible light irradiation. The key intermediates generated in situ in the cascade reaction have been tracked and identified. Studies using high-resolution mass spectrometry (HR-MS), UV-visible (UV-vis) absorption spectrum, electron spin resonance (ESR), x-ray absorption near-edge structure (XANES), and density functional theory (DFT) calculation reveal that simple Cu(II) salts associate with starting material of secondary amines **1** not only to activate the N–H bond and subsequently C–H bond but also to form new absorption species in the visible light region that is essential to ensure that the whole reaction proceeds in the absence of any external photosensitizer. Detailed mechanistic investigations suggest that the initial key step is a single-electron transfer from amine **1** to a Cu(II) ion, forming intermediate **I**, [Cu(I)-$NH^{+\bullet}$], that is, $NH^{+\bullet}$ of amine **1** and Cu(I). With visible light irradiation, the intermediate **I** reacts with oxygen (O_2) to generate singlet oxygen ($^1O_2$), which can oxidize the $NH^{+\bullet}$ of amine **1** into imine **4.** The imine **4** further coordinates with a Cu(II) ion to start the second stage of reaction, that is, a single-electron transfer from imine **4** to a Cu(II) ion, forming intermediate **II**, [Cu(I)-$N^{+\bullet}$], that is, $N^{+\bullet}$ of the imine **4** and Cu(I). As a result, the electrophilicity of imine **4** in intermediate **II** is increased for the subsequent nucleophilic addition (Scheme 1). In addition, molecule O_2 is beneficial for releasing the desired product and regenerating the Cu(II) ion to complete the catalytic cycle.

RESULTS AND DISCUSSION

Our initial study focused on the reaction of methyl 2-(4-methoxyphenylamino)acetate **1a** and indole **2a.** Typically, substrate **1a** and tert-butyloxycarbonyl (Boc)–protected **2a** were dissolved in MeCN and followed by addition of $Cu(OTf)_2$. The reaction mixture was then irradiated by blue light-emitting diodes (LEDs) at room temperature for 24 hours in air. Surprisingly, 50% yield of the cyclized product **3a** was obtained without any external photosensitizer (*37*, *38*). Because substrates **1a** and **2a** and Cu(II) salts show no absorption in the range of visible light, we believed that some new species formed in situ, which are responsible for this visible light–driven reaction. When Cu(II) salts were added, the solution of **1a** in MeCN turned from pale to red immediately, and new absorption peaks around 500 nm appeared (Fig. 1).

The interesting transformation prompted us to identify the new species formed in situ. Fortunately, HR-MS investigation provided direct evidence on the species. The peaks at 258.0182 and 451.0918 corresponding

[1]Key Laboratory of Photochemical Conversion and Optoelectronic Materials, Technical Institute of Physics and Chemistry and University of Chinese Academy of Sciences, Chinese Academy of Sciences, Beijing 100190, P. R. China. [2]Beijing Synchrotron Radiation Facility, Institute of High Energy Physics, Chinese Academy of Sciences, Beijing 100039, P. R. China.
*Corresponding author. Email: lzwu@mail.ipc.ac.cn

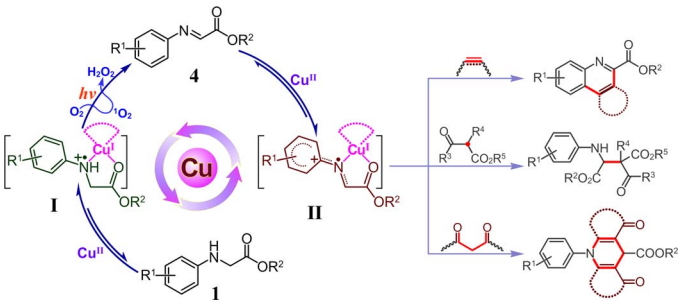

Scheme 1. Cu(II) salt–catalyzed C–H activation of secondary aromatic amines under visible light irradiation.

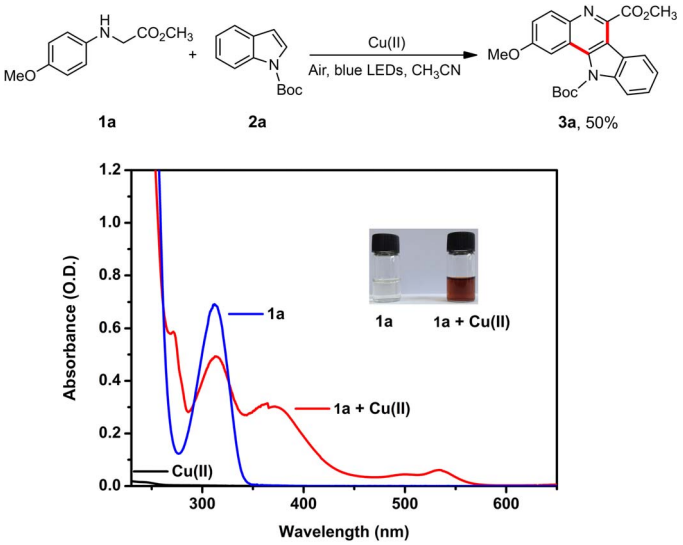

Fig. 1. UV-vis spectra of Cu(II) salts, 1a, and 1a with Cu(II) ion in MeCN. The concentration of Cu(II) ions is 9.0×10^{-5} M, and the concentration of **1a** is 3.0×10^{-4} M. The Cu(II) ion used here refers to $Cu(OTf)_2$. O.D., optical density.

to $[\mathbf{1a} + Cu]^{2+}$ and $[\mathbf{1a} + Cu + \mathbf{1a} - 2H]^{2+}$, respectively, were always detected regardless of the ratio of **1a** and Cu(II) salts (fig. S1). To monitor the oxidation states of copper in these species, we performed ESR and XANES experiments. As shown in Fig. 2, a typical peak for Cu(II) was detected when Cu(II) ions were dissolved in MeCN (Fig. 2A, red line) (*27*, *39*). However, this typical peak disappeared immediately upon addition of **1a** into the solution, suggesting that Cu(II) ions may interact with **1a** intimately to cause a change of oxidation state of copper. This assumption was further verified by the absorption edge of XANES. A typical feature was observed at lower energy (8.979 keV) corresponding to the 1s-3d of the Cu(II) complex (*40*, *41*), whereas a pre-edge at 8.984 keV originated from 1s-4p of Cu(I) indicated the occurrence of the single-electron transfer process upon addition of **1a** into the solution of Cu(II) ions in MeCN (Fig. 2B).

After adding **1a** into the solution of Cu(II) ions, new peaks that are assigned to $NH^{+\bullet}$ by computational simulation [$a_{NH}(N) = 6.16$ G; $a_{NH}(H) = 6.70$ G; $a_{CH2}(H) = 6.06$ G; $a_{ring\ 2,2'}(H) = 3.13$ G; $a_{ring\ 3,3'}(H) = 3.03$ G; fig. S3] (*42*) were simultaneously detected by ESR (Fig. 2A, black line, corresponding to the enlarged spectra shown in Fig. 2C). This signal increased in the first 2 min, remained unchanged for 1 min, and finally decreased gradually (fig. S4). From these results, we inferred that the simple Cu(II) ions associated with the starting material of secondary amine **1a**, leading to the occurrence of the single-electron transfer from **1a** to Cu(II) ion directly to afford intermediate **I** in the dark.

The identity of intermediate **I** was further confirmed by DFT calculation. As shown in Fig. 3A, four possible intermediates, that is, **I1** $[\mathbf{1a}\text{-}Cu]^{2+}$, **I2** $[\mathbf{1a}\text{-}Cu\text{-}\mathbf{1a}]^{2+}$, **I3** $[\mathbf{1a}\text{-}Cu\text{-}1MeCN]^{2+}$, and **I4** $[\mathbf{1a}\text{-}Cu\text{-}2MeCN]^{2+}$, were involved. The spin density distributions in **I1**, **I3**, and **I4** were mainly delocalized on **1a** (Fig. 3B), with negligible population on the center of Cu, although the spin density of Cu (0.52) in **I2** indicated that the single electron mainly populated on the center of Cu. The possible intermediates **I1**, **I3**, and **I4** involved single-electron transfer from **1a** to Cu(II) ion, which was in accordance with the observations supported by XANES and ESR experiments. Among the three possible intermediates, **I4** has the most favorable binding energy. Therefore, we speculated that Cu(I)-amine radical cation **I4** was the most possible intermediate between **1a** and Cu(II) ion.

However, the transformation reported in the current study hardly proceeded in the absence of light or air (Table 1, entries 8 and 9). This suggested that another oxygen active species contributed to the unique Cu(II) salt–catalyzed reaction under visible light irradiation. For the active species of oxygen, 2,2,6,6-tetramethyl piperidine (TEMP) and 5,5-dimethyl-1-pyrroline-*N*-oxide (DMPO) were used as probes to trap singlet oxygen ($^1O_2$) and superoxide radical anion ($O_2^{-\bullet}$), respectively, which could be easily detected by ESR spectroscopy (*43*, *44*). As discussed above, intermediate **I** formed in situ from **1a** and Cu(II) ion has the responsive ability to visible light. Upon irradiation of the solution of TEMP or DMPO, Cu(II) ions, and **1a** in air-saturated MeCN solution by visible light (λ = 450 nm; blue LEDs), a single radical was trapped, the spectrum and hyperfine coupling constants of which are consistent with the reported values of nitroxide radical 2,2,6,6-tetramethyl piperidinooxy (TEMPO) from $^1O_2$ and TEMP (Fig. 2D, red line), whereas the adduct of $O_2^{-\bullet}$ with DMPO was hardly detected (Fig. 2D, black line). Evidently, singlet oxygen $^1O_2$ was considered as the active species formed under irradiation of **1a** and Cu(II) ions. Singlet oxygen $^1O_2$ could oxidize amines into the corresponding imines (*45*). With visible light irradiation of **1a** and Cu(II) ions in air-saturated MeCN solution, 50% yield of imine **4a** was isolated (Scheme 2A), whereas no reaction occurred with the addition of specific singlet oxygen ($^1O_2$) quencher, that is, DABCO (1,4-diazabicyclo[2.2.2]octane) (*46*). The isolated imine **4a** could further react with nucleophile **2a** with the help of Cu(II) salts in the dark to yield 64% of indolo[3,2-*c*]quinoline product **3a** (Scheme 2B). Because no target product could be obtained in the absence of Cu(II) salts (Scheme 2C), Cu(II) salts should contribute to the outcome of this reaction.

Similar to that observed in the first stage for the formation of intermediate **I**, the association of imine **4a** with Cu(II) salts was detected. The peaks at 297.0299 and 449.0768 corresponding to $[\mathbf{4a} + Cu + MeCN]^{2+}$ and $[\mathbf{4a} + Cu + \mathbf{4a}]^{2+}$, respectively, were observed in HR-MS spectrometry (fig. S2). With the addition of Cu(II) salts into the MeCN solution of imine **4a**, the solution color changed from faint yellow to red, and the signal of Cu(II) ion in ESR spectra disappeared, accompanied by generation of a new one, probably derived from $N^{+\bullet}$ of imine (Fig. 2, E and F). Similar to intermediate **I**, the single-electron transfer from imine **4a** to Cu(II) ion occurred in intermediate **II**, that is, **II1** $[\mathbf{4a}\text{-}Cu]^{2+}$, **II2** $[\mathbf{4a}\text{-}Cu\text{-}\mathbf{4a}]^{2+}$, **II3** $[\mathbf{4a}\text{-}Cu\text{-}1MeCN]^{2+}$, and **II4** $[\mathbf{4a}\text{-}Cu\text{-}2MeCN]^{2+}$ (Fig. 4). Because the spin density of Cu in **II2** (0.61) or in **II4** (0.64) mainly populates on the Cu center, we speculated that Cu(I)-imine radical cation **II3** is the most possible intermediate. Given the higher conjugated effect

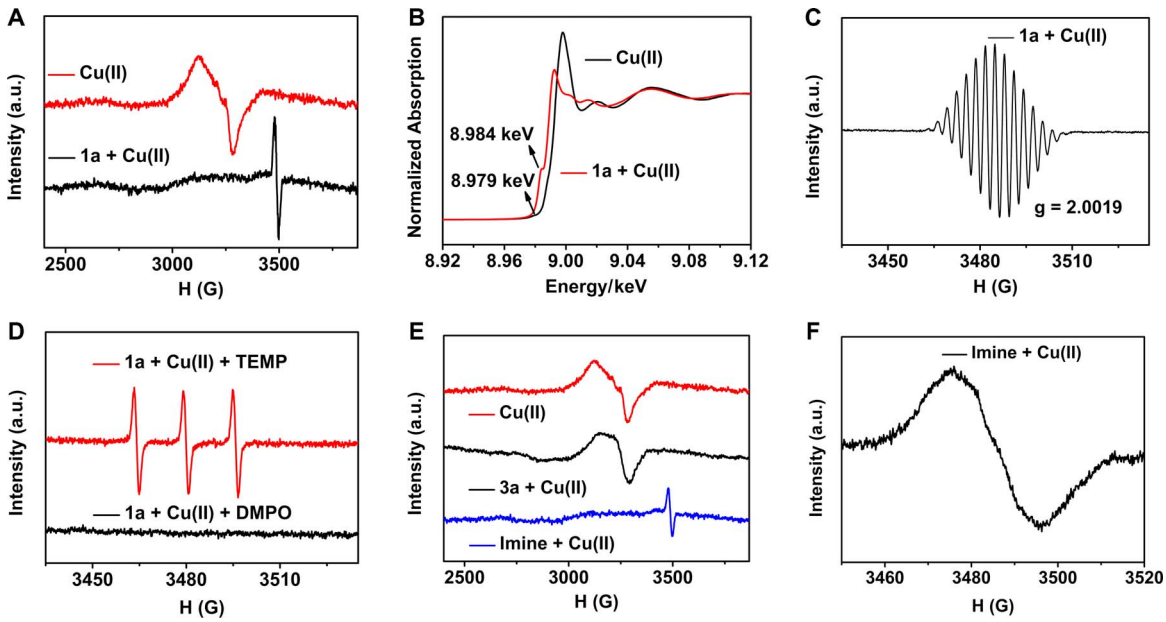

Fig. 2. Spectroscopic experiments. (**A**) ESR spectra of Cu(II) salts and the mixture of Cu(II) ion with **1a** in CH_3CN. (**B**) Normalized Cu XANES spectra of Cu(II) salts and **1a** with Cu(II) ion in CH_3CN. (**C**) ESR spectra of the mixture of Cu(II) ion with **1a** in CH_3CN (the enlarged spectra corresponding to the black line in **a**). (**D**) ESR spectra of an air-saturated CH_3CN solution of TEMP, Cu(II) ion, and **1a** or DMPO, Cu(II) ion, and **1a** upon irradiation for 30 s; both $NH^{+\bullet}$ signals of **1a** had been deducted. (**E**) ESR spectra of a solution of Cu(II) salts, **3a** with Cu(II) ion, and imine with Cu(II) ion in CH_3CN. (**F**) ESR spectra of the mixture of Cu(II) ion with imine in CH_3CN. The Cu(II) ion used here refers to $Cu(OTf)_2$.

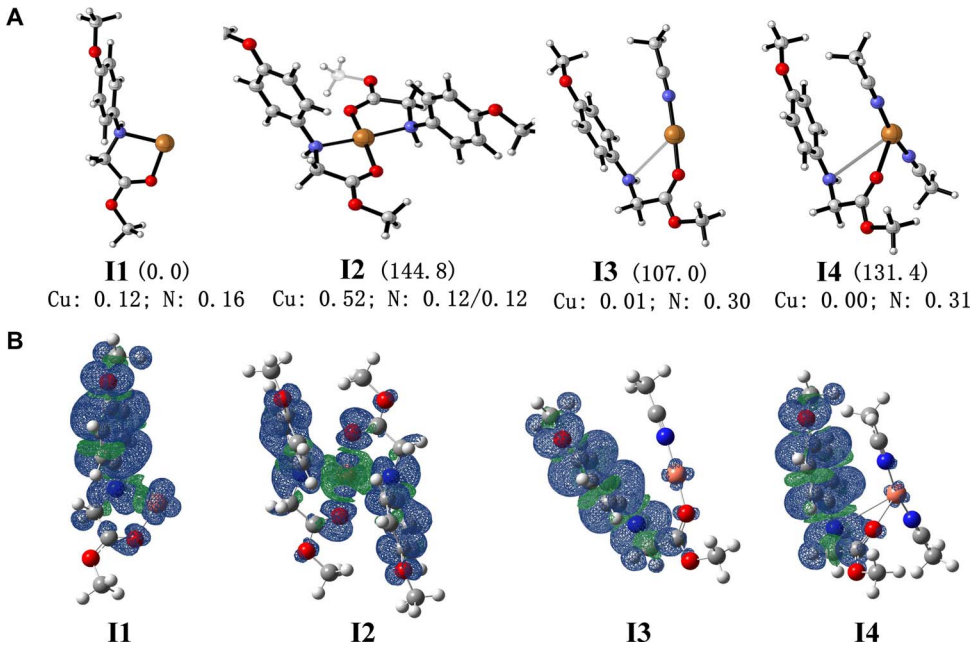

Fig. 3. Calculation studies of intermediate I. (**A**) Optimized geometrical structures of intermediate **I.** (**B**) Spin density distributions of **I1** [**1a**-Cu]$^{2+}$, **I2** [**1a**-Cu-**1a**]$^{2+}$, **I3** [**1a**-Cu-1MeCN]$^{2+}$, and **I4** [**1a**-Cu-2MeCN]$^{2+}$ at the B3LYP+GD3+CPCM/6-311+G** level. The related binding energy (in kilojoules per mole) and spin density of the key atoms (Cu and N of **1a**) are indicated in parentheses and at the bottom of the correspondence, respectively. [**1a**-Cu]$^{2+}$ was taken as a unit and the energy reference point.

of intermediate **II3** than intermediate **I4**, the spin density of N atom in **II3** markedly decreased.

On the basis of these results, we proposed that for the cascade photocatalytic process described herein, it is not only intermediate **I** of Cu(II) ion with **1a** and singlet oxygen $^1O_2$ oxidation for the formation of imine (*47*) but also intermediate **II** of Cu(II) ion with imine **4a** for the key bond-forming step of the product indolo[3,2-*c*]quinoline **3a** as an example shown in Scheme 3. The fact that (i) the oxidation state of Cu(II) remained unchanged in the presence of product **3a** (Fig. 2E, black line) and (ii) the signal of Cu(II) disappeared immediately when

Table 1. Impact of reaction parameters for the synthesis of indolo [3,2-*c*]quinoline 3a. Unless otherwise specified, the reaction was carried out with substrate **1** (0.25 mmol), **2** (0.1 mmol), and copper salts (0.03 mmol) in CH_2Cl_2 (2.5 ml) under irradiation with blue LEDs for 24 hours at room temperature.

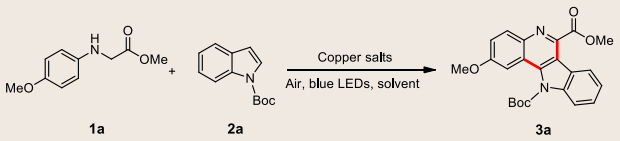

1a 2a 3a

Entry	Solvent	Copper salts	Yield (%)*
1	MeCN	$Cu(OTf)_2$	50
2	MeOH	$Cu(OTf)_2$	0
3	THF	$Cu(OTf)_2$	0
4	DMF	$Cu(OTf)_2$	0
5	$CHCl_3$	$Cu(OTf)_2$	32
6	CF_3-Ph	$Cu(OTf)_2$	20
7	CH_2Cl_2	$Cu(OTf)_2$	29
8†	MeCN	$Cu(OTf)_2$	5
9‡	MeCN	$Cu(OTf)_2$	0
10	MeCN	—	0
11	CH_2Cl_2	CuI	0
12	CH_2Cl_2	CuBr	0
13	CH_2Cl_2	$CuCl_2$	37
14	MeCN	CuI	0
15	MeCN	CuBr	0
16§	MeCN	$Cu(OTf)_2$	60
17¶	MeCN	$Cu(OTf)_2$	71

*Isolated yields after purification by column chromatography. †Carried out in the dark. ‡Under argon atmosphere. §Fifteen milligrams of 4 Å sieves was added. ¶**2a** was dissolved in MeCN and then injected into the solution for 10 min based on entry 14.

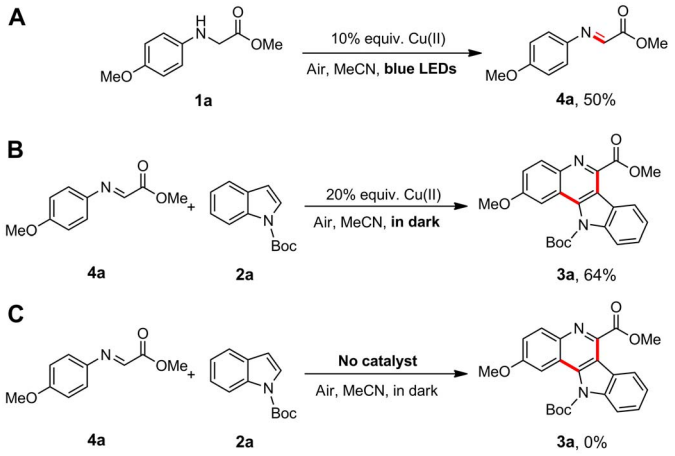

Scheme 2. Control experiments. (**A**) Reaction of **1a** in the absence of **2a** during the reaction. (**B**) The reaction of **4a** and **2a** was carried out in the dark. (**C**) The reaction of **4a** and **2a** was carried out without any catalyst.

excess amount of either amine **1a** or imine **4a** was presented in the solution of **3a** (Fig. 2E, blue line) indicated that the interaction of Cu(II) ion with **3a** was much weaker than that of its corresponding amine **1a** and imine **4a** in intermediate **I** and **II**, respectively. H_2O_2 was successfully detected as a by-product in the reaction mixture (see Materials and Methods) (*48*), suggesting that molecular O_2 could regenerate Cu(I) to Cu(II) in the following transformation of **6a** to **7a**, and Cu(II) ion released from **7a** into the solution would coordinate to another imine to complete the reaction cycle.

By considering that indolo[3,2-*c*]quinoline and quinoline are important structures of multitudinous natural products and biomolecules (*49*, *50*), we optimized reaction conditions and expanded the scope of this transformation. Screening reaction condition revealed that MeCN was the best choice (Table 1, entries 1 to 7), and $Cu(OTf)_2$ showed better performance than the other Cu(I) and Cu(II) salts for this transformation (Table 1, entries 10 to 15). Addition of 4 Å sieves into the reaction mixture resulted in enhanced reaction efficiency, suggesting that water influenced the transformation to some extent (Table 1, entry 16). Progressive addition of **2a** into the solution significantly improved the yield of product **3** to 71% (Table 1, entry 17). Either electron-donating (Me) or electron-withdrawing groups (F, Cl, or Br) at the para-position of aryl amines **1** were tolerated (Table 2, entries 2 to 5). Notably, crystal structure of product **3b** confirmed the formation of indolo[3,2-*c*]quinolines other than indolo[2,3-*c*]quinolines (fig. S5). Compared to para-substituents, meta-substituted aryl amine gave lower efficiency (Table 2, entry 6). It is of significance that the intramolecular cyclization underwent selectively at the para-position of bromo group rather than at its ortho-position. In addition to methyl ester of the amine, all ethyl-, tert-butyl–, and benzyl-substituted secondary amines **1** were compatible with this reaction (Table 2, entries 7 to 9). In particular, products **3** containing chloro and bromo functionalities can serve as potential intermediates for further transformation. Moreover, a wide range of Boc-protected indoles were able to react with amines **1.** Overall, electron-donating groups showed better performance than electron-withdrawing groups regardless of 5- or 6-substituted indole derivatives (Table 2, entries 10 to 14). Next, we evaluated the cascade reaction of amines **1** with other nucleophiles such as arynes or aromatic olefins **8** (*51*–*53*). Satisfactorily, all of them could proceed with moderate yields. Increasing the electron density of aromatic rings would be beneficial for the transformation (Table 3).

As a further extension, a series of *N*-substituted glycine esters bearing electron-donating or electron-withdrawing groups in the para-position of phenyl ring coupled with 2-oxocyclopentanecarboxylate **10** were studied (*54*–*56*). Most of them could be successfully transformed into desired product **11** in good to excellent yields (Table 4, entries 1 to 6). β-Ketoesters **10** have also a wide range of applicability under the standard conditions. Substituted methyl, ethyl, sterically bulky isopropyl, and tert-butyl as well as benzyl groups are compatible with this protocol, affording excellent yields of products (Table 4, entries 7 to 15). Even the less reactive acyclic β-ketoester could undergo direct alkylation, albeit with a moderate yield (Table 4, entry 16).

Unexpectedly, when 2,4-pentanedione **12a** was used as the nucleophile, trace amount of product could be obtained within 1 hour of irradiation. However, when the reaction time was extended to 12 hours, 1,4-dihydropyridine **13a** was isolated as yellow solids at room temperature (scheme S1A). The reaction parameters were optimized for the synthesis of 1,4-dihydropyridine **13a** shown in Table 5. With the use of β-ketoester **10a** to replace β-diketone **12a**, the same situation

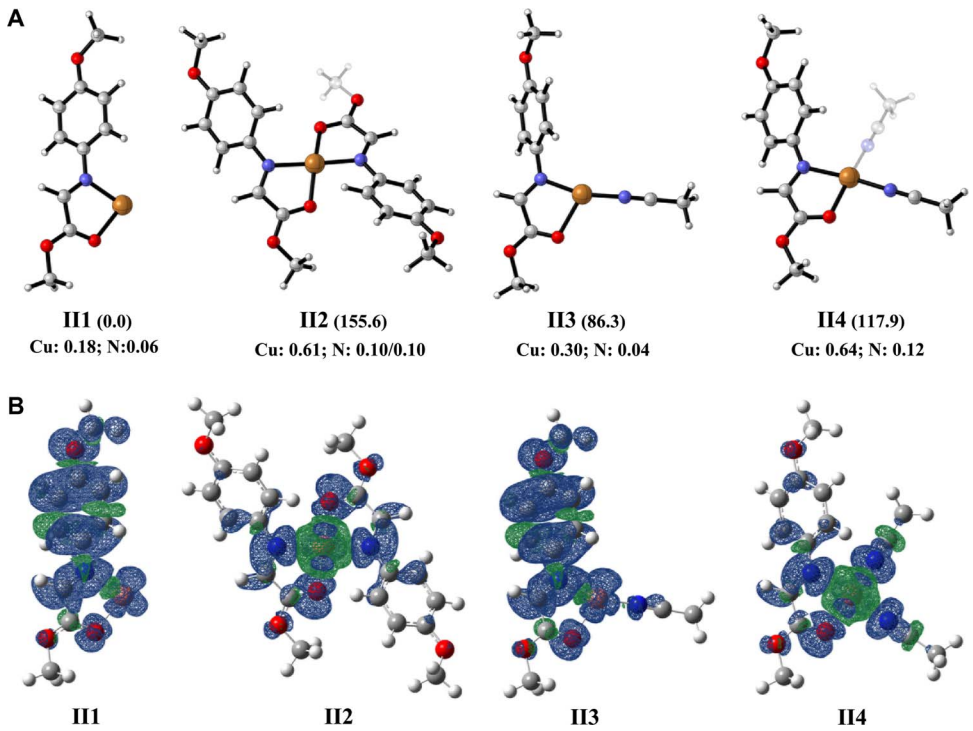

Fig. 4. Calculation studies of intermediate II. (**A**) Optimized geometrical structures of intermediate **II.** (**B**) Spin density distributions of **II1** [**4a**-Cu]$^{2+}$, **II2** [**4a**-Cu-**4a**]$^{2+}$, **II3** [**4a**-Cu-1MeCN]$^{2+}$, and **II4** [**4a**-Cu-2MeCN]$^{2+}$ at the B3LYP+GD3+CPCM/6-311+G** level. The related binding energy (in kilojoules per mole) and spin density of the key atoms (Cu and N of **4a**) are indicated in parentheses and at the bottom of the correspondence, respectively. [**4a**-Cu]$^{2+}$ was taken as a unit and the energy reference point.

did not appear. This is different from the case observed in the cascade reaction between secondary amines and β-ketoesters catalyzed by tris(4-bromophenyl)aminium hexachloroantimonate (*57*). Reaction of imine **4a** with 2,4-pentanedione **12a** afforded the corresponding 1,4-dihydropyridine **13a**, further demonstrating the significance of imine **4a** formed in the first stage of the Cu(II) salt–catalyzed cascade reaction (scheme S1B). Monitoring ^{1}H nuclear magnetic resonance (NMR) spectra revealed that the produced imine **4a** decomposed slowly into its corresponding aromatic amine **14a** and aldehyde **15a.** The former (**14a**) could condense with one molecule of β-diketone to yield enamine **17a**, and the latter (**15a**) was quickly transformed into α,β-unsaturated ketoester **16a.** Finally, intermolecular Michael addition of **16a** and **17a** as well as intramolecular condensation released the product of 1,4-dihydropyridine **13a** (Scheme 4) (*58*, *59*).

As illustrated in Table 6, a variety of secondary amines with different esters could produce 1,4-dihydroyridines **13a** to **13d** in good yields. In addition to methoxy-substituted aromatic ring, methyl, fluoro, and bromo groups also functioned well to produce **13e** to **13h** in moderate yields. Replacing acetylacetone with unsymmetric β-diketones, such as 2,4-hexanedione and 1-phenyl-1,3-butanedione as the coupling partners, yielded 1,4-dihydropyridine **13i** and **13j** in 60 and 72% yields, respectively. In addition, cyclic β-diketones were well tolerated to produce fused ring compounds **13k** and **13l** in moderate yields.

CONCLUSION

In summary, we have demonstrated that Cu(II) salts enable C–H functionalization of aromatic amines to directly form a variety of C–C bonds in air without any external photosensitizer under visible light irradiation at room temperature. A range of quinoline, indolo [3,2-*c*]quinoline, β-amino acid, and 1,4-dihydropyridine derivatives have been achieved in moderate to good chemical yields. An array of mechanistic studies reveals that the simple Cu(II) ion associates with secondary amine by single-electron transfer to form visible light absorption intermediate **I** [Cu(I)-NH$^{+\bullet}$]. Immediately, the N–H and C–H bonds of the amine are activated and further transformed into the corresponding imine by $^1O_2$, generated by irradiation of intermediate **I** [Cu(I)-NH$^{+\bullet}$] with O_2 under visible light. Next, intermediate **II** [Cu(I)-N$^{+\bullet}$] is produced by the single-electron transfer from the imine to Cu(II) ion in the second stage, which increases electrophilicity of the imine for the following addition with nucleophiles. Identifying these key intermediates in the cascade aerobic reaction will facilitate the exploration and exploitation of potential application of Cu(II) salts in synthetic chemistry, thereby leading to lower-cost, milder, and greener processes for catalytic transformations.

MATERIALS AND METHODS

^{1}H NMR spectra were recorded using a Bruker Avance DPX 400 MHz instrument with tetramethylsilane as an internal standard. ^{13}C NMR spectra were obtained at 100 MHz and referenced to the internal solvent signals. HR-MS (ESI) spectra were recorded on a Fourier transform ion cyclotron resonance mass spectrometer at the Analytical Instrumentation Center, Peking University. Steady-state emission spectra were recorded using a PerkinElmer LS50B spectrofluorometer. ESR spectra were recorded at room temperature using a Bruker ESP-300E spectrometer at 9.8 GHz, X-band, with 100-Hz field modulation. X-ray absorption spectroscopic (XANES measurements) data were collected at beamlines 1W1B and 1W2B of the Beijing Synchrotron Radiation Facility (BSRF). All reactions were carried out under air. MeCN was

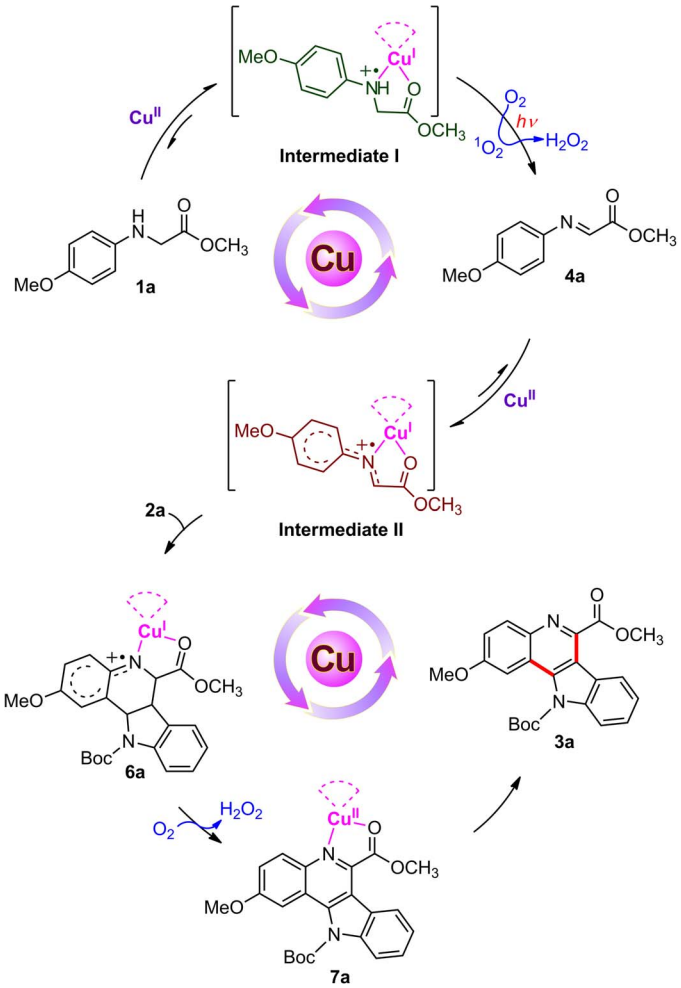

Scheme 3. Proposed catalytic cycle for the synthesis of indolo[3,2-*c*]quinoline 3a under visible light irradiation.

dried by anhydrous $MgSO_4$ before use. Irradiation was carried out with blue LED (3 W). Sieves (4 Å) were activated in a muffle furnace at 250°C for 2 hours. Commercially available reagents were used without further purification.

General procedure for the reaction of aryl amine and Boc-protected indole derivatives

A 10-ml Pyrex tube equipped with a magnetic stir bar was charged with aryl amine (0.25 mmol), $Cu(OTf)_2$ (0.03 mmol), MeCN (2.5 ml), and 15 mg of 4 Å sieves. Boc-protected indole derivative (0.1 mmol) in 0.5 ml of MeCN was slowly injected for 10 min under irradiation with blue LEDs at room temperature. Then, the solution was stirred for another 30 hours under irradiation with blue LEDs at room temperature. Finally, the mixture was evaporated under reduced pressure to remove the solvents, and the residue was purified by flash chromatography on silica gel to afford the desired product.

General procedure for the reaction of aryl amines and alkene or alkyne derivatives

A 10-ml Pyrex tube equipped with a magnetic stir bar was charged with aryl amines (0.2 mmol), alkene or alkyne derivatives (0.1 mmol), and

Table 2. Reaction scope for the synthesis of indolo[3,2-*c*]quinoline derivatives. Unless otherwise noted, reactions were run with substrate **1** (0.25 mmol), $Cu(OTf)_2$ (0.03 mmol), and 15 mg of 4 Å sieves in 2.5 ml of MeCN, and **2** (0.1 mmol) in 0.5 ml of MeCN was injected into the solution for 10 min under irradiation with blue LEDs at room temperature.

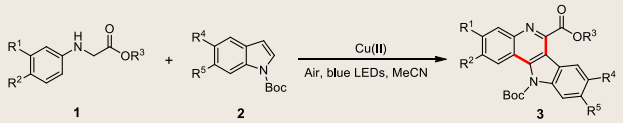

1 2 3

Entry	R^1	R^2	R^3	R^4	R^5	Product	
						3	Yield (%)*
1	H	OMe	Me	H	H	**3a**	71
2	H	Me	Me	H	H	**3b**	78
3	H	F	Me	H	H	**3c**	52
4	H	Cl	Me	H	H	**3d**	80
5	H	Br	Me	H	H	**3e**	71
6	Br	H	Me	H	H	**3f**	34
7	H	OMe	Et	H	H	**3g**	73
8	H	OMe	t-Bu	H	H	**3h**	68
9	H	OMe	Benzyl	H	H	**3i**	65
10	H	Me	Me	H	Me	**3j**	76
11	H	Me	Me	H	Cl	**3k**	53
12	H	Me	Me	Me	H	**3l**	71
13	H	Me	Me	OMe	H	**3m**	76
14	H	Me	Me	Br	H	**3n**	34

*Isolated yields after purification by column chromatography.

Table 3. Reaction scope for the synthesis of quinoline derivatives under visible light irradiation. Unless otherwise noted, reaction was carried out with **1a** (0.25 mmol), arynes or aromatic olefins **8** (0.1 mmol), and $Cu(OTf)_2$ (0.01 mmol) in 3 ml of MeCN under irradiation with blue LEDs at room temperature.

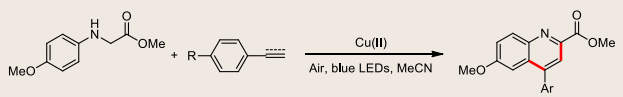

1a 8 9

Entry	R	Product		
		9	Ar	Yield (%)*
1†	H	**9a**	Ph	45
2†	OMe	**9b**	4-MeOPh	52
3†	F	**9c**	4-FPh	36
4‡	H	**9a**	Ph	40
5‡	OMe	**9b**	4-MeOPh	50
6‡	F	**9c**	4-FPh	32

*Isolated yields after purification by column chromatography. †Arynes. ‡Aromatic olefins.

Table 4. Reaction scope for the synthesis of β-amino acid derivatives under visible light irradiation. Unless otherwise noted, reactions were carried out with substrate **1** (0.2 mmol), **10** (0.1 mmol), and $Cu(OTf)_2$ (0.01 mmol) in 3 ml of MeCN under irradiation with blue LEDs at room temperature. d.r., diastereomeric ratio.

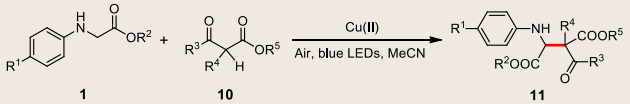

1 10 11

Entry	R^1	R^2	R^3	R^4	R^5	Product		
						11	d.r.	Yield (%)*
1	OMe	Me	$(CH_2)_3$		Et	**11a**	1.8:1	90
2	OMe	Et	$(CH_2)_3$		Et	**11b**	2:1	87
3	OMe	Benzyl	$(CH_2)_3$		Et	**11c**	3:1	70
4	Cl	Et	$(CH_2)_3$		Et	**11d**	2.3:1	64
5	Br	Et	$(CH_2)_3$		Et	**11e**	2.4:1	67
6	Me	Et	$(CH_2)_3$		Et	**11f**	1.1:1	84
7	OMe	Me	$(CH_2)_3$		Me	**11g**	1.2:1	83
8	OMe	Et	$(CH_2)_3$		Me	**11h**	1.5:1	93
9	OMe	Me	$(CH_2)_3$		i-Pr	**11i**	3:1	91
10	OMe	Et	$(CH_2)_3$		i-Pr	**11j**	2.3:1	94
11	OMe	Et	$(CH_2)_3$		t-Bu	**11k**	1.9:1	83
12	OMe	Me	$(CH_2)_3$		t-Bu	**11l**	1.8:1	84
13	OMe	Et	$(CH_2)_3$		Benzyl	**11m**	2:1	72
14	OMe	Me	Ph	H	Et	**11n**	1.2:1	81
15	OMe	Et	Ph	H	Et	**11o**	1.2:1	85
16	OMe	Et	Ph	Me	Et	**11p**	1:1	55

*Isolated yields after purification by column chromatography.

Table 5. Impact of reaction parameters for the synthesis of 1,4-dihydropyridine 13a. Unless otherwise specified, the reaction was carried out with substrate **1a** (0.1 mmol), **12a**, and $Cu(OTf)_2$ in MeCN under irradiation with blue LEDs at room temperature.

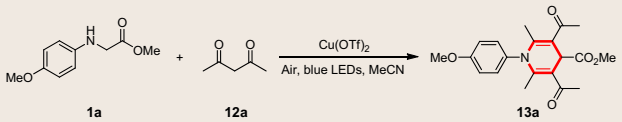

1a 12a 13a

Entry	12a (mmol)	$Cu(OTf)_2$ (mmol)	MeCN (ml)	Yield (%)*
1	0.2	0.02	2	21
2	0.3	0.02	2	40
3	0.4	0.02	2	47
4	0.5	0.02	2	50
5	0.75	0.02	2	51
6	1	0.02	2	50
7	0.5	0.02	6	35
8	0.5	0.02	8	29
9	0.5	0.02	1	55
10	0.5	0.02	0.5	48
11	0.5	0.01	1	35
12	0.5	0.03	1	52
13†	0.5	0.02	1	67

*Isolated yields after purification by column chromatography. †After the reaction was finished, 1 equiv. of $NaBH_3CN$ was added and stirred for 1 hour.

$Cu(OTf)_2$ (0.02 mmol) in MeCN (3 ml) under irradiation with blue LEDs for 6 hours at room temperature. Then, the reaction mixture was evaporated under reduced pressure to remove the solvents, and the residue was purified by flash chromatography on silica gel to afford the desired product.

General procedure for the reaction of aryl amine and β-ketoester derivatives

A 10-ml Pyrex tube equipped with a magnetic stir bar was charged with aryl amine (0.2 mmol), β-ketoester (0.1 mmol), and $Cu(OTf)_2$ (0.01 mmol) in MeCN (3 ml) under irradiation with blue LEDs for 1 hour at room temperature. Then, the mixture was evaporated under reduced pressure to remove the solvents, and the residue was purified by flash chromatography on silica gel to afford the desired product.

General procedure for the reaction of aryl amine and β-diketone derivatives

A 10-ml Pyrex tube equipped with a magnetic stir bar was charged with aryl amine (0.2 mmol), β-diketone (0.5 mmol), and $Cu(OTf)_2$ (0.04 mmol) in MeCN (2 ml) under irradiation with blue LEDs at room temperature. After completion monitored by thin-layer chromatography analysis, the mixture was evaporated under reduced pressure to remove the solvents, and the residue was purified by flash chromatography on silica gel to afford the desired product.

Procedures for ESR experiments

The sample of $Cu(OTf)_2$ (1.6×10^{-2} M), **1a** (6.4×10^{-2} M), and imine (6.4×10^{-2} M) in MeCN was prepared. For detection of Cu(II) ions, the solution of $Cu(OTf)_2$ was diluted to 8.0×10^{-3} M with MeCN, and then an aliquot of the solution was transferred into an ESR tube. ESR spectrum was recorded at room temperature using 1500-Hz field modulation. For detection of N radical cation, an equivalent amount of $Cu(OTf)_2$ (1.6×10^{-2} M) solution was mixed with **1a** (6.4×10^{-2} M) or imine (6.4×10^{-2} M), and then an aliquot of the solution was transferred into an ESR tube. ESR spectrum was recorded at room temperature using 100-Hz field modulation. For the detection of superoxide radical anion ($O_2^{-\bullet}$), an aliquot of the solution sample containing DMPO (2.0×10^{-2} M), $Cu(OTf)_2$ (1.25×10^{-4} M), **1a** (1.25×10^{-3} M), or imine (1.25×10^{-3} M) in air-saturated MeCN was transferred into an ESR tube. Upon irradiation for 30 s, ESR spectrum was recorded at room temperature using 100-Hz field modulation. For detection of singlet oxygen ($^1O_2$), TEMP (0.12 M) was used to replace DMPO. $NH^{+\bullet}$ signal of **1a** was simulated by WinESR software (see below) to yield the hyperfine splitting constants $a_{NH}(N) = 6.16$ G, $a_{NH}(H) = 6.70$ G, $a_{CH2}(H) = 6.06$ G, $a_{ring\ 2,2'}(H) = 3.13$ G, and $a_{ring\ 3,3'}(H) = 3.03$ G.

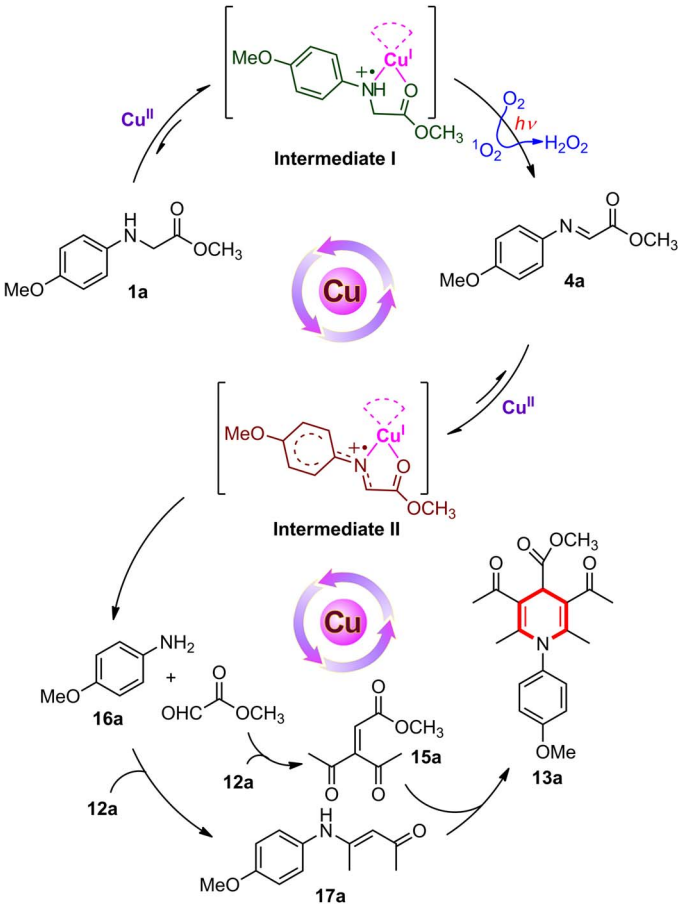

Scheme 4. Proposed catalytic cycle for the synthesis of 1,4-dihydropyridine 13a under visible light irradiation.

Table 6. Reaction scope for the synthesis of 1,4-dihydropyridine derivatives. Unless otherwise noted, reactions were run with **1** (0.1 mmol), **12** (0.5 mmol), and $Cu(OTf)_2$ (0.02 mmol) in 1 ml of MeCN under irradiation with blue LEDs at room temperature.

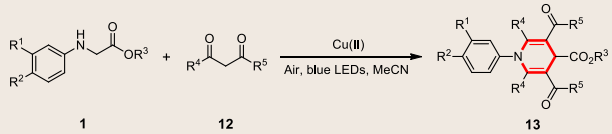

Entry	R^1	R^2	R^3	R^4	R^5	Product 13	Yield (%)*
1	H	OMe	Me	Me	Me	**13a**	67
2	H	OMe	Et	Me	Me	**13b**	68
3	H	OMe	Benzyl	Me	Me	**13c**	61
4	H	OMe	t-Bu	Me	Me	**13d**	59
5	H	Me	Me	Me	Me	**13e**	51
6	Me	H	Me	Me	Me	**13f**	35
7	H	F	Me	Me	Me	**13g**	51
8	H	Br	Me	Me	Me	**13h**	32
9	H	OMe	Me	Me	Et	**13i**	60
10	H	OMe	Me	Me	Ph	**13j**	72
11	H	OMe	Me	$(CH_2)_3$		**13k**	54
12	H	OMe	Me	$[CH_2C(CH_3)_2CH_2]$		**13l**	57

*Isolated yields after purification by column chromatography.

X-ray absorption spectroscopy experiments

X-ray absorption measurements (XANES) were performed at beamlines 1W1B and 1W2B of the BSRF. The data were collected in transmission and fluorescence quick scan mode. The ionization chambers were optimized for the maximal current with linear response (10^{10} photons detected per second) with 10% absorption (N_2) in the incident ion chamber and 70% absorption (60% N_2 and 40% Ar) in the incident, transmission, and fluorescent x-ray detector. The samples of $Cu(OTf)_2$ (1.5×10^{-2} M) and **1a** (0.1 M) with $Cu(OTf)_2$ (1.5×10^{-2} M) in MeCN were prepared.

DFT calculations

The DFT (*60*, *61*) method B3LYP hybrid functional (*62*, *63*) in combination with the 6-311+G** basis set was used to optimize two series of possible intermediates. One involves **1a**, Cu(II) ion, and CH_3CN; the other includes **4a**, Cu(II) ion, and MeCN. During optimization, the solvent effect was considered via a self-consistent reaction field method based on the conductor-like polarizable continuum model (CPCM) (*64*, *65*) for MeCN, and the dispersion effect was considered with the Grimme's D3 version (GD3) (*66*). The frequency analysis validated all optimized structures as the real minima. All calculations were performed with the Gaussian 09 software package (*67*).

On the basis of the optimized structures, we calculated the related binding energy and spin density. Here, the Gibbs free energy at 298.15 K and 1.0 atm was used to calculate the binding energy. In **1a** with Cu(II) ion in MeCN, $[\mathbf{1a}\text{-Cu}]^{2+}$ was referred as a unit, and the binding energy of $[\mathbf{1a}\text{-Cu-}\mathbf{1a}]^{2+}$ ($[\mathbf{1a}\text{-Cu-1MeCN}]^{2+}$) was defined as the Gibbs free energy difference between $[\mathbf{1a}\text{-Cu-}\mathbf{1a}]^{2+}$ ($[\mathbf{1a}\text{-Cu-1MeCN}]^{2+}$) and $[\mathbf{1a}\text{-Cu}]^{2+}$ with **1a**; the binding second MeCN energy for $[\mathbf{1a}\text{-Cu-1MeCN}]^{2+}$ was the Gibbs free energy difference between $[\mathbf{1a}\text{-Cu-2MeCN}]^{2+}$ and $[\mathbf{1a}\text{-Cu-1MeCN}]^{2+}$ with MeCN. The total binding energy of $[\mathbf{1a}\text{-Cu-2MeCN}]^{2+}$ was the sum of $[\mathbf{1a}\text{-Cu}]^{2+}$ binding two MeCN by two steps. Similar to **1a** with Cu(II) ion in MeCN, we calculated the binding energies of possible intermediates in **4a** with Cu(II) in MeCN. In combination with the experimental ESR and XANES studies, we proposed the two most possible intermediate **I** (**I4**) and intermediate **II** (**II3**) at the different reaction stage.

Detection of H_2O_2

After the reaction was completed, 5 ml of CH_2Cl_2 was added, the resulting solution was filtered, and 2 ml of saturated aqueous solution of sodium carbonate was introduced into the solution to extract H_2O_2. Then, 35 ml of isopropanol solution containing 2.5 ml of glacial acetic acid and 2 g of sodium iodide was injected into the extracted H_2O_2 aqueous solution and heated to reflux for 5 min. In the course of the heating process, the solution color became yellow, featuring H_2O_2 formation (*48*).

SUPPLEMENTARY MATERIALS

Supplementary material for this article is available at http://advances.sciencemag.org/cgi/content/full/3/8/e1700666/DC1

Characterization data for all compounds

^{1}H and ^{13}C NMR
Cartesian coordinates (Å) and Gibbs free energies (Hartree) of all optimized structures
fig. S1. ESI HR-MS for the mixture of **1a** and Cu(II) ions.
fig. S2. ESI HR-MS for the mixture of imine and Cu(II) ions.
fig. S3. ESR spectrum of $Cu(OTf)_2$ and **1a** in MeCN.
fig. S4. ESR experiments for variation of radical $NH^{+\bullet}$ with the change of time.
fig. S5. X-ray crystal structure of **3b**.
scheme S1. Cu(II) salt–catalyzed reactions for the synthesis of 1,4-dihydropyridine **13a**.

REFERENCES AND NOTES

1. A. E. Wendlandt, A. M. Suess, S. S. Stahl, Copper-catalyzed aerobic oxidative C–H functionalizations: Trends and mechanistic insights. *Angew. Chem. Int. Ed.* **50**, 11062–11087 (2011).
2. C. Zhang, C. Tang, N. Jiao, Recent advances in copper-catalyzed dehydrogenative functionalization via a single electron transfer (SET) process. *Chem. Soc. Rev.* **41**, 3464–3484 (2012).
3. S. A. Girard, T. Knauber, C.-J. Li, The cross-dehydrogenative coupling of C_{sp3}–H bonds: A versatile strategy for C–C bond formations. *Angew. Chem. Int. Ed.* **53**, 74–100 (2014).
4. X.-X. Guo, D.-W. Gu, Z. Wu, W. Zhang, Copper-catalyzed C–H functionalization reactions: Efficient synthesis of heterocycles. *Chem. Rev.* **115**, 1622–1651 (2015).
5. J. Xuan, W.-J. Xiao, Visible-light photoredox catalysis. *Angew. Chem. Int. Ed.* **51**, 6828–6838 (2012).
6. D. A. Nicewicz, T. M. Nguyen, Recent applications of organic dyes as photoredox catalysts in organic synthesis. *ACS Catal.* **4**, 355–360 (2013).
7. D. P. Hari, B. König, The photocatalyzed Meerwein arylation: Classic reaction of aryl diazonium salts in a new light. *Angew. Chem. Int. Ed.* **52**, 4734–4743 (2013).
8. C. K. Prier, D. A. Rankic, D. W. C. MacMillan, Visible light photoredox catalysis with transition metal complexes: Applications in organic synthesis. *Chem. Rev.* **113**, 5322–5363 (2013).
9. M. D. Kärkäs, J. A. Porco, C. R. J. Stephenson, Photochemical approaches to complex chemotypes: Applications in natural product synthesis. *Chem. Rev.* **116**, 9683–9747 (2016).
10. K. L. Skubi, T. R. Blum, T. P. Yoon, Dual catalysis strategies in photochemical synthesis. *Chem. Rev.* **116**, 10035–10074 (2016).
11. M. Pirtsch, S. Paria, T. Matsuno, H. Isobe, O. Reiser, $[Cu(dap)_2Cl]$ as an efficient visible-light-driven photoredox catalyst in carbon–carbon bond-forming reactions. *Chem. Eur. J.* **18**, 7336–7340 (2012).
12. A. C. Hernandez-Perez, A. Vlassova, S. K. Collins, Toward a visible light mediated photocyclization: Cu-based sensitizers for the synthesis of [5]helicene. *Org. Lett.* **14**, 2988–2991 (2012).
13. S. Paria, M. Pirtsch, V. Kais, O. Reiser, Visible-light-induced intermolecular atom-transfer radical addition of benzyl halides to olefins: Facile synthesis of tetrahydroquinolines. *Synthesis* **45**, 2689–2698 (2013).
14. A. Baralle, L. Fensterbank, J.-P. Goddard, C. Ollivier, Aryl radical formation by copper(I) photocatalyzed reduction of diaryliodonium salts: NMR evidence for a Cu^{II}/Cu^{I} mechanism. *Chem. Eur. J.* **19**, 10809–10813 (2013).
15. A. C. Hernandez-Perez, S. K. Collins, A visible-light-mediated synthesis of carbazoles. *Angew. Chem. Int. Ed.* **52**, 12696–12700 (2013).
16. S. Paria, O. Reiser, Copper in photocatalysis. *ChemCatChem* **6**, 2477–2483 (2014).
17. Z. Zhang, X. Tang, C. S. Thomoson, W. R. Dolbier Jr., Photoredox-catalyzed intramolecular aminodifluoromethylation of unactivated alkenes. *Org. Lett.* **17**, 3528–3531 (2015).
18. X.-J. Tang, W. R. Dolbier Jr., Efficient Cu-catalyzed atom transfer radical addition reactions of fluoroalkylsulfonyl chlorides with electron-deficient alkenes induced by visible light. *Angew. Chem. Int. Ed.* **54**, 4246–4249 (2015).
19. M. Knorn, T. Rawner, R. Czerwieniec, O. Reiser, [Copper(phenanthroline)(bisisonitrile)]$^+$-complexes for the visible-light-mediated atom transfer radical addition and alkylation reactions. *ACS Catal.* **5**, 5186–5193 (2015).
20. D. B. Bagal, G. Kachkovskyi, M. Knorn, T. Rawner, B. M. Bhanage, O. Reiser, Trifluoromethylchlorosulfonylation of alkenes: Evidence for an inner-sphere mechanism by a copper phenanthroline photoredox catalyst. *Angew. Chem. Int. Ed.* **54**, 6999–7002 (2015).
21. G. Fumagalli, P. T. G. Rabet, S. Boyd, M. F. Greaney, Three-component azidation of styrene-type double bonds: Light-switchable behavior of a copper photoredox catalyst. *Angew. Chem. Int. Ed.* **54**, 11481–11484 (2015).
22. A. C. Hernandez-Perez, A. Caron, S. K. Collins, Photochemical synthesis of complex carbazoles: Evaluation of electronic effects in both UV- and visible-light methods in continuous flow. *Chem. Eur. J.* **21**, 16673–16678 (2015).
23. T. P. Nicholls, G. E. Constable, J. C. Robertson, M. G. Gardiner, A. C. Bissember, Brønsted acid cocatalysis in copper(I)-photocatalyzed α-amino C–H bond functionalization. *ACS Catal.* **6**, 451–457 (2016).
24. P. T. G. Rabet, G. Fumagalli, S. Boyd, M. F. Greaney, Benzylic C–H azidation using the Zhdankin reagent and a copper photoredox catalyst. *Org. Lett.* **18**, 1646–1649 (2016).
25. T. Rawner, M. Knorn, E. Lutsker, A. Hossain, O. Reiser, Synthesis of trifluoromethylated sultones from alkenols using a copper photoredox catalyst. *J. Org. Chem.* **81**, 7139–7147 (2016).
26. O. Reiser, Shining light on copper: Unique opportunities for visible-light-catalyzed atom transfer radical addition reactions and related processes. *Acc. Chem. Res.* **49**, 1990–1996 (2016).
27. S. E. Creutz, K. J. Lotito, G. C. Fu, J. C. Peters, Photoinduced Ullmann C–N coupling: Demonstrating the viability of a radical pathway. *Science* **338**, 647–651 (2012).
28. A. C. Bissember, R. J. Lundgren, S. E. Creutz, J. C. Peters, G. C. Fu, Transition-metal-catalyzed alkylations of amines with alkyl halides: Photoinduced, copper-catalyzed couplings of carbazoles. *Angew. Chem. Int. Ed.* **52**, 5129–5133 (2013).
29. C. Uyeda, Y. Tan, G. C. Fu, J. C. Peters, A new family of nucleophiles for photoinduced, copper-catalyzed cross-couplings via single-electron transfer: Reactions of thiols with aryl halides under mild conditions (0°C). *J. Am. Chem. Soc.* **135**, 9548–9552 (2013).
30. D. T. Ziegler, J. Choi, J. M. Muñoz-Molina, A. C. Bissember, J. C. Peters, G. C. Fu, A versatile approach to Ullmann C–N couplings at room temperature: New families of nucleophiles and electrophiles for photoinduced, copper-catalyzed processes. *J. Am. Chem. Soc.* **135**, 13107–13112 (2013).
31. H.-Q. Do, S. Bachman, A. C. Bissember, J. C. Peters, G. C. Fu, Photoinduced, copper-catalyzed alkylation of amides with unactivated secondary alkyl halides at room temperature. *J. Am. Chem. Soc.* **136**, 2162–2167 (2014).
32. Y. Tan, J. M. Muñoz-Molina, G. C. Fu, J. C. Peters, Oxygen nucleophiles as reaction partners in photoinduced, copper-catalyzed cross-couplings: *O*-arylations of phenols at room temperature. *Chem. Sci.* **5**, 2831–2835 (2014).
33. T. S. Ratani, S. Bachman, G. C. Fu, J. C. Peters, Photoinduced, copper-catalyzed carbon–carbon bond formation with alkyl electrophiles: Cyanation of unactivated secondary alkyl chlorides at room temperature. *J. Am. Chem. Soc.* **137**, 13902–13907 (2015).
34. A. Sagadevan, A. Ragupathi, C.-C. Lin, J. R. Hwu, K. C. Hwang, Visible-light initiated copper(I)-catalysed oxidative C–N coupling of anilines with terminal alkynes: One-step synthesis of α-ketoamides. *Green Chem.* **17**, 1113–1119 (2015).
35. W.-J. Yoo, T. Tsukamoto, S. Kobayashi, Visible light-mediated Ullmann-type C–N coupling reactions of carbazole derivatives and aryl iodides. *Org. Lett.* **17**, 3640–3642 (2015).
36. Q. M. Kainz, C. D. Matier, A. Bartoszewicz, S. L. Zultanski, J. C. Peters, G. C. Fu, Asymmetric copper-catalyzed C-N cross-couplings induced by visible light. *Science* **351**, 681–684 (2016).
37. Z.-Q. Wang, M. Hu, X.-C. Huang, L.-B. Gong, Y.-X. Xie, J.-H. Li, Direct α-arylation of α-amino carbonyl compounds with indoles using visible light photoredox catalysis. *J. Org. Chem.* **77**, 8705–8711 (2012).
38. S. Zhu, M. Rueping, Merging visible-light photoredox and Lewis acid catalysis for the functionalization and arylation of glycine derivatives and peptides. *Chem. Commun.* **48**, 11960–11962 (2012).
39. E. I. Solomon, Spectroscopic methods in bioinorganic chemistry: Blue to green to red copper sites. *Inorg. Chem.* **45**, 8012–8025 (2006).
40. L. S. Kau, D. J. Spira-Solomon, J. E. Penner-Hahn, K. O. Hodgson, E. I. Solomon, X-ray absorption edge determination of the oxidation state and coordination number of copper. Application to the type 3 site in *Rhus vernicifera* laccase and its reaction with oxygen. *J. Am. Chem. Soc.* **109**, 6433–6442 (1987).
41. C. He, G. Zhang, J. Ke, H. Zhang, J. T. Miller, A. J. Kropf, A. Lei, Labile Cu(I) catalyst/spectator Cu(II) species in copper-catalyzed C–C coupling reaction: Operando IR, in situ XANES/EXAFS evidence and kinetic investigations. *J. Am. Chem. Soc.* **135**, 488–493 (2013).
42. P. D. Josephy, T. Eling, R. P. Mason, The horseradish peroxidase-catalyzed oxidation of 3,5,3′,5′-tetramethylbenzidine. Free radical and charge-transfer complex intermediates. *J. Biol. Chem.* **257**, 3669–3675 (1982).
43. J. Ma, J. Zhao, L. Jiang, Effect of structural modification on photodynamic activity of hypocrellins. *Photochem. Photobiol.* **74**, 143–148 (2001).
44. F. A. Villamena, Y. Liu, J. L. Zweier, Superoxide radical anion adduct of 5,5-dimethyl-1-pyrroline *N*-oxide. 4. Conformational effects on the EPR hyperfine splitting constants. *J. Phys. Chem. A* **112**, 12607–12615 (2008).
45. G. Jiang, J. Chen, J.-S. Huang, C.-M. Che, Highly efficient oxidation of amines to imines by singlet oxygen and its application in Ugi-type reactions. *Org. Lett.* **11**, 4568–4571 (2009).
46. E. Baciocchi, T. Del Giacco, F. Elisei, M. F. Gerini, M. Guerra, A. Lapi, P. Liberali, Electron transfer and singlet oxygen mechanisms in the photooxygenation of dibutyl sulfide and thioanisole in MeCN sensitized by *N*-methylquinolinium tetrafluoborate and 9,10-dicyanoanthracene. The probable involvement of a thiadioxirane intermediate in electron transfer photooxygenations. *J. Am. Chem. Soc.* **125**, 16444–16454 (2003).
47. T. Daimon, Y. Nosaka, Formation and behavior of singlet molecular oxygen in TiO_2 photocatalysis studied by detection of near-infrared phosphorescence. *J. Phys. Chem. C* **111**, 4420–4424 (2007).

48. R. D. Mair, A. J. Graupner, Determination of organic peroxides by iodine liberation procedures. *Anal. Chem.* **36**, 194–204 (1964).
49. A. Paulo, E. T. Gomes, P. J. Houghton, New alkaloids from *Cryptolepis sanguinolenta*. *J. Nat. Prod.* **58**, 1485–1491 (1995).
50. S. Van Miert, S. Hostyn, B. U. W. Maes, K. Cimanga, R. Brun, M. Kaiser, P. Mátyus, R. Dommisse, G. Lemière, A. Vlietinck, L. Pieters, Isoneocryptolepine, a synthetic indoloquinoline alkaloid, as an antiplasmodial lead compound. *J. Nat. Prod.* **68**, 674–677 (2005).
51. H. Richter, O. García Mancheño, TEMPO oxoammonium salt-mediated dehydrogenative Povarov/oxidation tandem reaction of N-alkyl anilines. *Org. Lett.* **13**, 6066–6069 (2011).
52. C. Huo, Y. Yuan, M. Wu, X. Jia, X. Wang, F. Chen, J. Tang, Auto-oxidative coupling of glycine derivatives. *Angew. Chem. Int. Ed.* **53**, 13544–13547 (2014).
53. C. Huo, H. Xie, M. Wu, X. Jia, X. Wang, F. Chen, J. Tang, CBr_4-mediated cross-dehydrogenative coupling reaction of amines. *Chem. Eur. J.* **21**, 5723–5726 (2015).
54. G. Zhang, Y. Zhang, R. Wang, Catalytic asymmetric activation of a C_{sp^3}–H bond adjacent to a nitrogen atom: A versatile approach to optically active α-alkyl α-amino acids and C1-alkylated tetrahydroisoquinoline derivatives. *Angew. Chem. Int. Ed.* **50**, 10429–10432 (2011).
55. X.-W. Gao, Q.-Y. Meng, M. Xiang, B. Chen, K. Feng, C.-H. Tung, L.-Z. Wu, Combining visible light catalysis and transition metal catalysis for the alkylation of secondary amines. *Adv. Synth. Catal.* **355**, 2158–2164 (2013).
56. X.-W. Gao, Q.-Y. Meng, J.-X. Li, J.-J. Zhong, T. Lei, X.-B. Li, C.-H. Tung, L.-Z. Wu, Visible light catalysis assisted site-specific functionalization of amino acid derivatives by C–H bond activation without oxidant: Cross-coupling hydrogen evolution reaction. *ACS Catal.* **5**, 2391–2396 (2015).
57. X. Jia, Y. Wang, F. Peng, C. Huo, L. Yu, J. Liu, X. Wang, Catalytic oxidation of C(sp^3)–H bonds induced by a radical cation salt: Construction of 1,4-dihydropyridines using a fragment-reassembly strategy. *Adv. Synth. Catal.* **356**, 1210–1216 (2014).
58. W. Shen, L.-M. Wang, H. Tian, J. Tang, J.-j. Yu, Brønsted acidic imidazolium salts containing perfluoroalkyl tails catalyzed one-pot synthesis of 1,8-dioxo-decahydroacridines in water. *J. Fluorine Chem.* **130**, 522–527 (2009).
59. Y.-p. Liu, J.-m. Liu, X. Wang, T.-m. Cheng, R.-t. Li, Multicomponent reactions leading to symmetric and asymmetric multi-substituted 1,4-dihydropyridines on montmorillonite. *Tetrahedron* **69**, 5242–5247 (2013).
60. R. G. Parr, W. Yang, *Density-Functional Theory of Atoms and Molecules* (Oxford Univ. Press, 1989).
61. C. J. Cramer, D. G. Truhlar, Density functional theory for transition metals and transition metal chemistry. *Phys. Chem. Chem. Phys.* **11**, 10757–10816 (2009).
62. A. D. Becke, Density-functional thermochemistry. III. The role of exact exchange. *J. Chem. Phys.* **98**, 5648–5652 (1993).
63. C. Lee, W. Yang, R. G. Parr, Development of the Colle-Salvetti correlation-energy formula into a functional of the electron density. *Phys. Rev. B* **37**, 785–789 (1988).
64. V. Barone, M. Cossi, Quantum calculation of molecular energies and energy gradients in solution by a conductor solvent model. *J. Phys. Chem. A* **102**, 1995–2001 (1998).
65. M. Cossi, N. Rega, G. Scalmani, V. Barone, Energies, structures, and electronic properties of molecules in solution with the C-PCM solvation model. *J. Comput. Chem.* **24**, 669–681 (2003).
66. S. Grimme, J. Antony, S. Ehrlich, H. Krieg, A consistent and accurate ab initio parametrization of density functional dispersion correction (DFT-D) for the 94 elements H-Pu. *J. Chem. Phys.* **132**, 154104 (2010).
67. M. J. Frisch, G. W. Trucks, H. B. Schlegel, G. E. Scuseria, M. A. Robb, J. R. Cheeseman, G. Scalmani, V. Barone, B. Mennucci, G. A. Petersson, H. Nakatsuji, M. Caricato, X. Li, H. P. Hratchian, A. F. Izmaylov, J. Bloino, G. Zheng, J. L. Sonnenberg, M. Hada, M. Ehara, K. Toyota, R. Fukuda, J. Hasegawa, M. Ishida, T. Nakajima, Y. Honda, O. Kitao, H. Nakai, T. Vreven, J. A. Montgomery Jr., J. E. Peralta, F. Ogliaro, M. Bearpark, J. J. Heyd, E. Brothers, K. N. Kudin, V. N. Staroverov, T. Keith, R. Kobayashi, J. Normand, K. Raghavachari, A. Rendell, J. C. Burant, S. S. Iyengar, J. Tomasi, M. Cossi, N. Rega, J. M. Millam, M. Klene, J. E. Knox, J. B. Cross, V. Bakken, C. Adamo, J. Jaramillo, R. Gomperts, R. E. Stratmann, O. Yazyev, A. J. Austin, R. Cammi, C. Pomelli, J. W. Ochterski, R. L. Martin, K. Morokuma, V. G. Zakrzewski, G. A. Voth, P. Salvador, J. J. Dannenberg, S. Dapprich, A. D. Daniels, O. Farkas, J. B. Foresman, J. V. Ortiz, J. Cioslowski, D. J. Fox, *Gaussian 09, Revision E.01* (Gaussian Inc., 2013).
68. L.-Z. Wu, Q.-Y. Meng, T. Lei, X.-W. Gao, J.-J. Zhong, M. Xiang, B. Chen, C.-H. Tung, Chinese Patent 201310001383.X (2013).

Acknowledgments

Funding: This work was supported by the Ministry of Science and Technology of China (2013CB834804, 2013CB834505, and 2014CB239402), the National Natural Science Foundation of China (21390404, 91427303, 21473227, and 21402217), the Strategic Priority Research Program of the Chinese Academy of Sciences (XDB17030400), and the Chinese Academy of Sciences. **Author contributions:** L.-Z.W. and Q.-Y.M. devised the initial concept of the work and designed the experiments. Q.-Y.M. and X.-W.G. contributed to the synthesis of products and mechanism investigation. T.L. and Z.L. performed the synthesis of starting materials and characterized the products. F.Z., Z.-J.L., and Y.T. performed x-ray absorption experiments. H.X. performed theoretical calculation. L.-Z.W. and Q.-Y.M. wrote the manuscript. J.-J.Z., K.F., B.C., and C.-H.T. helped with the discussion and analysis of the data. **Competing interests:** L.-Z.W., Q.-Y.M., T.L., X.-W.G., J.-J.Z., B.C., and C.-H.T. are authors on a patent related to this paper (Chinese Patent 201310001383.X, 2013) (*68*). M. Xiang is also an author on this patent, but is not an author of this paper. All other authors declare that they have no competing interests. **Data and materials availability:** All data needed to evaluate the conclusions in the paper are present in the paper and/or the Supplementary Materials. Additional data related to this paper may be requested from L.-Z.W. (lzwu@mail.ipc.ac.cn).

Submitted 7 March 2017
Accepted 1 August 2017
Published 25 August 2017
10.1126/sciadv.1700666

Citation: Q.-Y. Meng, X.-W. Gao, T. Lei, Z. Liu, F. Zhan, Z.-J. Li, J.-J. Zhong, H. Xiao, K. Feng, B. Chen, Y. Tao, C.-H. Tung, L.-Z. Wu, Identifying key intermediates generated in situ from Cu(II) salt–catalyzed C–H functionalization of aromatic amines under illumination. *Sci. Adv.* **3**, e1700666 (2017).